

Structures of the first and second double-stranded RNA-binding domains of human TAR RNA-binding protein

Seisuke Yamashita,^{1,2} Takashi Nagata,¹ Masahito Kawazoe,¹ Chie Takemoto,¹ Takanori Kigawa,^{1,3} Peter Güntert,^{1,4,5} Naohiro Kobayashi,¹ Takaho Terada,¹ Mikako Shirouzu,¹ Motoaki Wakiyama,¹ Yutaka Muto,^{1*} and Shigeyuki Yokoyama^{1,2*}

¹RIKEN Systems and Structural Biology Center, 1-7-22 Suehiro-cho, Tsurumi, Yokohama 230-0045, Japan

²The University of Tokyo, 7-3-1 Hongo, Bunkyo, Tokyo 113-0033, Japan

³Tokyo Institute of Technology, 4259 Nagatsuta-cho, Midori-ku, Yokohama 226-8502, Japan

⁴Tatsuo Miyazawa Memorial Program, RIKEN Genomic Sciences Center, Yokohama 230-0045, Japan

⁵Institute of Biophysical Chemistry and Frankfurt Institute of Advanced Studies, Goethe University Frankfurt, 60438 Frankfurt am Main, Germany

Received 27 October 2010; Accepted 29 October 2010

DOI: 10.1002/pro.543

Published online 15 November 2010 proteinscience.org

Abstract: The TAR RNA-binding Protein (TRBP) is a double-stranded RNA (dsRNA)-binding protein, which binds to Dicer and is required for the RNA interference pathway. TRBP consists of three dsRNA-binding domains (dsRBDs). The first and second dsRBDs (dsRBD1 and dsRBD2, respectively) have affinities for dsRNA, whereas the third dsRBD (dsRBD3) binds to Dicer. In this study, we prepared the single domain fragments of human TRBP corresponding to dsRBD1 and dsRBD2 and solved the crystal structure of dsRBD1 and the solution structure of dsRBD2. The two structures contain an α - β - β - β - α fold, which is common to the dsRBDs. The overall structures of dsRBD1 and dsRBD2 are similar to each other, except for a slight shift of the first α helix. The residues involved in dsRNA binding are conserved. We examined the small interfering RNA (siRNA)-binding properties of these dsRBDs by isothermal titration calorimetry measurements. The dsRBD1 and dsRBD2 fragments both bound to siRNA, with dissociation constants of 220 and 113 nM, respectively. In contrast, the full-length TRBP and its fragment with dsRBD1 and dsRBD2 exhibited much smaller dissociation constants (0.24 and 0.25 nM, respectively), indicating that the tandem dsRBDs bind simultaneously to one siRNA molecule. On the other hand, the loop between the first α helix and the first β strand of dsRBD2, but not dsRBD1, has a Trp residue, which forms hydrophobic and cation- π interactions with the surrounding residues. A circular dichroism analysis revealed that the thermal stability of dsRBD2 is higher than that of dsRBD1 and depends on the Trp residue.

Keywords: NMR; X-ray crystallographic study; structural genomics; solution structure; TAR-RNA binding protein; dsRBD

Abbreviations: dsRBD, double-stranded RNA binding domain; dsRNA, double-stranded RNA; HSQC, heteronuclear single quantum coherence; miRNA, microRNA; NOE, nuclear Overhauser effect; NOESY, NOE spectroscopy TRBP, TAR RNA-binding protein; siRNA, small interfering RNA

Seisuke Yamashita and Takashi Nagata contributed equally to this work.

Grant sponsors: Targeted Proteins Research Program (TPRP) and RIKEN Structural Genomics/Proteomics Initiative (RSGI), National Project on Protein Structural and Functional Analyses of the Ministry of Education, Culture, Sports, Science and Technology of Japan (MEXT).

*Correspondence to: Yutaka Muto, RIKEN Systems and Structural Biology Center, 1-7-22 Suehiro, Tsurumi, Yokohama 230-0045, Japan. E-mail: ymuto@gsc.riken.jp (or) Shigeyuki Yokoyama, RIKEN Systems and Structural Biology Center, 1-7-22 Suehiro, Tsurumi, Yokohama 230-0045, Japan. E-mail: yokoyama@biochem.s.u-tokyo.ac.jp

Introduction

RNA interference (RNAi) is an evolutionarily conserved gene silencing mechanism, which uses 21–23 nucleotide small RNAs for target RNA determination. There are two major classes of small RNAs involved in RNAi, micro RNA (miRNA) and small interfering RNA (siRNA). miRNAs are derived from pre-miRNA hairpins and have mismatches in the duplex, whereas siRNAs are derived from long dsRNAs and have no mismatches in the duplex.¹ These small RNA duplexes are generated by Dicer, an RNase III enzyme.² Humans have a single Dicer species, which generates both miRNAs and siRNAs, whereas other organisms have multiple Dicer species for different substrates.^{3,4} These small RNA duplexes are loaded into Argonaute (Ago), which is the effector protein of the RNA-induced silencing complex and are then separated into single strands.^{5,6} Only one strand of the duplex is retained by Ago, and it causes the cleavage (siRNA) or translational suppression (miRNA) of the complementary target RNA.^{1,7}

In many organisms, Dicer binds partner proteins with double-stranded RNA-binding domains (dsRBDs).⁸ In human, the partner proteins are the TAR RNA-binding protein (TRBP) and its homologous protein, PACT.^{9–11} TRBP was initially identified by its affinity for HIV TAR RNA and was subsequently revealed to participate in RNAi.¹² TRBP consists of three dsRBDs. The first and second dsRBDs (dsRBD1 and dsRBD2, respectively) have similar amino acid sequences and can bind dsRNA.¹³ In contrast, the third dsRBD (dsRBD3) lacks several of the conserved RNA-binding residues. Therefore, dsRBD3 cannot bind RNA but binds to Dicer.^{10,14,15}

It has been suggested that TRBP promotes the RNAi pathway. TRBP facilitates small RNA production by stabilizing Dicer and/or upregulating its enzymatic activity, whereas human Dicer can cleave substrate RNAs without TRBP.^{16–18} Moreover, the Dicer·TRBP complex may pass the produced siRNA duplex on to Ago.^{9,10,19,20} In this function of TRBP, the interactions of the TRBP dsRBD1 and dsRBD2 with siRNA are important, as TRBP binds siRNA more efficiently than Dicer.^{9,20} The single-particle EM structure of the complex of Dicer, TRBP, and Ago2 (a member of the Ago family) was reported, and the mechanisms of siRNA transfer from Dicer to Ago2 were discussed.²¹ Recently, the crystal structure of the complex between the TRBP dsRBD2 and dsRNA was reported and revealed the manner of canonical RNA-binding by dsRBD2.²²

In this study, we determined the crystal structure of dsRBD1 and the solution structure of dsRBD2. Our results indicated that dsRBD1 is quite similar to dsRBD2, with respect to the tertiary structure and the manner of dsRNA-binding without

a conformational change. An isothermal titration calorimetry (ITC) analysis revealed that the two dsRBDs simultaneously bind to an siRNA molecule to achieve high affinity. Furthermore, a circular dichroism (CD) analysis showed that the thermal stability of dsRBD2 is higher than that of dsRBD1, in which the evolutionarily “sporadic” tryptophan residue in dsRBD2 plays an important role.

Results and Discussion

The tertiary structures of the dsRBD1 and dsRBD2 fragments from human TRBP

We prepared the dsRBD1 and dsRBD2 fragments derived from human TRBP [Fig. 1(A)]. The amino acid sequences of these two dsRBDs [Fig. 1(B)] share 35% identity and 45% similarity. The structure of dsRBD1 was solved by X-ray crystallography [Fig. 1(C)], whereas that of dsRBD2 was determined by NMR spectroscopy [Fig. 1(D)]. Both dsRBD1 and dsRBD2 have an α - β - β - α fold, in which the two α helices pack against one face of the three-stranded antiparallel β sheet, a common feature of the dsRBDs [Fig. 1(B)].²³ The overall structures of the two dsRBDs are also similar to each other, except for a slight shift of the first α helix (α 1 helix) [Fig. 1(E)]. The root mean square deviation (RMSD) between the dsRBD1 and dsRBD2 structures was 1.2 Å for 56 C α atoms. Both dsRBD fragments are monomeric in the determined structures, in agreement with their gel filtration chromatography profiles (data not shown).

Comparison with the structure of the human TRBP dsRBD2-dsRNA complex

The present solution structure of the dsRBD2 fragment [Fig. 1(D)] was compared with the previously reported crystal structure of a human TRBP dsRBD2 fragment in complex with a nicked dsRNA²² [Fig. 2(A)]. The RNA-free and RNA-bound structures of dsRBD2 superposed well on each other (RMSD of 0.8 Å for 63 C α atoms) [Fig. 2(B)]. Therefore, the TRBP dsRBD2 binds dsRNA without any particular conformational change, in a similar manner as other dsRBDs.^{28,29} The overall structure of dsRBD2 in complex with dsRNA also resembles that of dsRBD1 (RMSD of 0.9 Å for 54 C α atoms), but the above-mentioned shift of the α 1 helix is still characteristic of the dsRBD1 structure, when compared with the RNA-free and RNA-bound dsRBD2 structures. The RNA-binding residues in dsRBD2 are well conserved in dsRBD1 [Fig. 2(C)]. Therefore, we built a dsRNA docking model of dsRBD1 [Fig. 2(D)], on the basis of the dsRBD2-dsRNA complex structure. The residues with side chains that directly interact with dsRNA in the dsRBD2-dsRNA complex, and the corresponding residues in dsRBD1, are shown in stick representations in Figure 2(A,D), respectively. In the

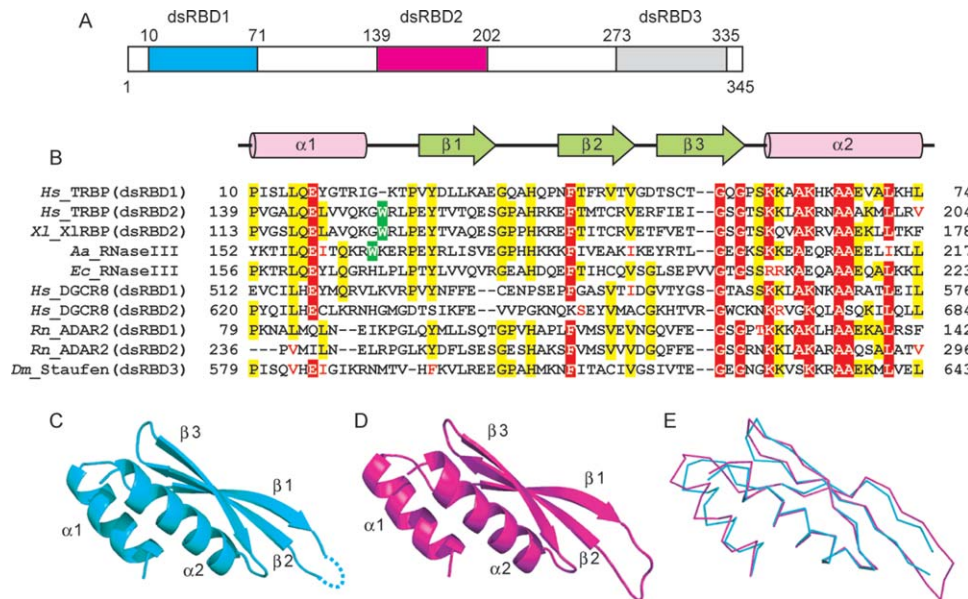


Figure 1. Structures of the dsRBD1 and dsRBD2 fragments from human TRBP. (A) Schematic diagram of human TRBP. (B) Sequence alignment of various dsRBDs. The dsRBD sequences from *H. sapiens* (*Hs*) TRBP (dsRBD1 and dsRBD2), *X. laevis* (*Xl*) XLRBP²⁴ (dsRBD2), *A. aeolicus* (*Aa*) RNase III,²⁵ *E. coli* (*Ec*) RNase III, *Hs* DGCR8²⁶ (dsRBD1 and dsRBD2), *R. norvegicus* (*Rn*) ADAR2²⁷ (dsRBD1 and dsRBD2), and *D. melanogaster* (*Dm*) Staufen^{22,23} (dsRBD3) are aligned, based on the secondary structures. Identical residues are shaded in red or yellow. Similar residues are shown with red letters. The secondary structure elements are represented with pink cylinders (α helices) and green arrows (β strands). The Trp152 residue in the TRBP dsRBD2 and its equivalent in the *Xl* XLRBP dsRBD2 are shaded in green. (C, D) Ribbon representations of the crystal structure of dsRBD1 (C) and the NMR structure of dsRBD2 (D) from human TRBP. Residues 15–81 in dsRBD1 and residues 138–205 in dsRBD2 are shown. Residues 35–37 in dsRBD1 were invisible. The N- and C-terminal ends of this loop section are connected by a dotted line. (E) Superimposition of the structures of dsRBD1 (cyan) and dsRBD2 (magenta).

docking model of dsRBD1, the side chains of Gln14, Glu15, Lys59, and Lys63 are modified so that they point in the same directions as those of Gln144, Glu145, Lys189, and Lys193 in dsRBD2, respectively. By contrast, the dsRBD2-dsRNA complex structure and the docking model of the dsRBD1-dsRNA complex exhibited two differences that might affect the RNA-binding of the dsRBDs. One is the shift of the $\alpha 1$ helix, and the other is the replacement of Arg194 in dsRBD2 by His64 in dsRBD1. However, as shown in Figure 2(D), the expected dsRNA-binding residues in dsRBD1, Gln14, and Glu15 are located sufficiently near the dsRNA and are therefore expected to interact with the dsRNA in a similar manner to Gln144 and Glu145, respectively. On the other hand, the side chain of His64 in dsRBD1 is oriented toward the dsRNA and seems to interact with it [Fig. 2(E)]. Therefore, dsRBD1 and dsRBD2 are expected to bind dsRNA in a similar manner, although their affinities may differ to some extent.

ITC measurements

We measured the affinities of dsRBD1 and dsRBD2 for siRNA, using various fragments of human TRBP (Fig. 3). Because the RNA affinities of single dsRBD fragments from human TRBP had been examined only with the TAR RNA,¹³ it was unclear whether dsRBD1 and/or dsRBD2 bound siRNA, which is

shorter and structurally simpler than the TAR RNA. In this study, ITC experiments were performed, by titration of the protein solution into the siRNA solution. The data were analyzed according to a one-site binding model, on the assumption that the multiple dsRBDs can bind one siRNA molecule independently and simultaneously. The generated curves fit well to the experimental data (Fig. 4). The dissociation constant (K_d) of the wild-type dsRBD1 fragment (D1-WT) and that of the wild-type dsRBD2 fragment (D2-WT) were 220 and 113 nM, respectively, and their stoichiometry factors were both ~ 2 [Figs. 3 and 4(A,B)]. The twofold stronger affinities of the dsRBD2 may be derived from the structural variations between the two fragments, as described above. The reported K_d values of dsRBD1 and dsRBD2 for the TAR RNA are about 8 μ and 59 nM, respectively.¹³ Thus, the affinities of dsRBD1 for these two RNA species are quite different, whereas those of dsRBD2 are similar to each other. dsRBD1 may be sensitive to the tertiary structures, such as the bulges or mismatches present in the TAR RNA or may have been affected by the different experimental conditions (ITC versus gel-shift assay or His-tag versus MBP-tag).

Next, we generated triple point mutants of the dsRBD fragments: His37, Lys59, and Lys63 in dsRBD1 and His167, Lys189, and Lys193 in dsRBD2,

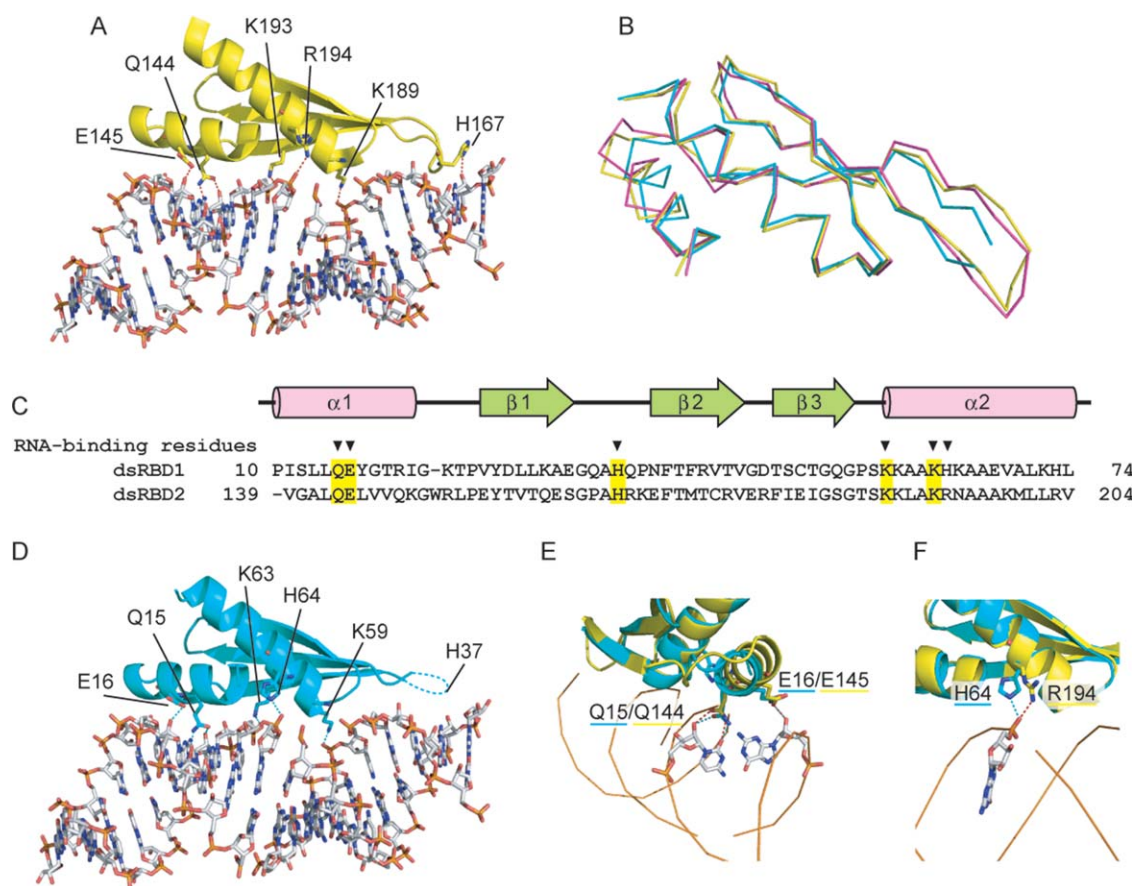


Figure 2. Comparison of the dsRNA-binding surfaces of the dsRBDs. (A) Structure of the TRBP dsRBD2-dsRNA complex²⁰ (PDB ID: 3ADL). The residues with side chains that directly interact with dsRNA are shown in stick representations. The hydrogen bonds are shown by dashed lines. (B) Superimposition of the dsRBD structures of dsRBD1 (cyan), and the RNA-free and RNA-bound structures of dsRBD2 (magenta and yellow, respectively). (C) Sequence alignment of dsRBD1 and dsRBD2 of TRBP. The dsRNA-binding residues are indicated with arrowheads. The conserved dsRNA-binding residues are shaded in yellow. (D) Docking model of the TRBP dsRBD1 with dsRNA. (E, F) Detailed views of the dsRNA-binding surfaces.

all were mutated to Ala (D1-mutant and D2-mutant, respectively) [Figs. 2(C) and 3]. As discussed above, these residues are expected to bind dsRNA and are conserved in dsRBD1 and dsRBD2. For both dsRBD fragments, the triple mutation abolished the affinity for siRNA [Figs. 3 and 4(C,D)]. The triple mutation was also introduced into dsRBD1 and/or dsRBD2 in the full-length protein. The full-length TRBP with the triple mutant dsRBD2 (FL-M2) and the full-length TRBP with the triple mutant dsRBD1 (FL-M1) have the wild-type dsRBD1 and dsRBD2, respectively, and showed similar binding patterns to those of D1-WT and D2-WT, respectively [Figs. 3 and 4(E,F)]. Consequently, the presence of the other two domains does not interfere with dsRBD1 or dsRBD2. The titration of the full-length TRBP with the triple mutations in both dsRBD1 and dsRBD2 (FL-M12) did not yield any detectable binding heat, which is consistent with the inability of dsRBD3 to bind dsRNA^{14,15} [Figs. 3 and 4(G)].

Interestingly, the heat change profile of the wild-type full-length TRBP (FL-WT) was different

from those of the other proteins containing one or no active dsRBDs and indicated the two modes of binding [Figs. 3 and 4(E)]. Therefore, we analyzed the data using a two-site binding model and obtained a well-fitted curve. The K_d values for the first and second binding modes were 0.24 and 13.3 nM, respectively. The stoichiometry factors for both were ~ 1 . The dsRBD3-deleted mutant (D12-WT) showed the similar two-mode binding manner to that of FL-WT. The K_d values for the two binding modes were 0.25 and 121 nM, respectively, and the stoichiometry factors for both modes were ~ 1 [Figs. 3 and 4(I)]. The affinity of the dsRBD3-deleted TRBP for siRNA in our experiment was similar to the previously reported value (0.77 nM).¹⁵ These quite small K_d values and the stoichiometry factors of ~ 1 in the first binding mode indicate that dsRBD1 and dsRBD2 in TRBP simultaneously bind to one siRNA molecule and enhance the affinity for siRNA, independently of dsRBD3. An siRNA molecule with 19 base pairs appears to lack sufficient room for both dsRBDs of the second protein molecule to bind


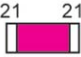

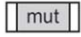
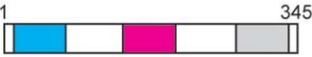

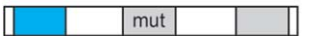
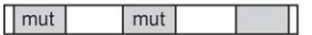
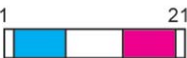
	Protein constructs			K_d (nM)	Stoichiometry factors
	dsRBD1	dsRBD2	dsRBD3		
D1- WT				220	1.85
D2- WT				113	2.43
D1- mutant				No binding	–
D2- mutant				No binding	–
FL- WT				0.24 (K_d1) 13.3 (K_d2)	1.01 0.91
FL- M1				201	2.47
FL- M2				486	1.95
FL- M12				No binding	–
D12- WT				0.25 (K_d1) 121 (K_d2)	1.13 1.19

Figure 3. ITC measurements. The list of the K_d values and the stoichiometry factors of the various TRBP constructs. For FL-WT and D12-WT, the K_d values for the first and second binding modes are represented by K_d1 and K_d2 , respectively. The triple mutations of H37A, K59A, and K63A in dsRBD1 and those of H167A, K189A, and K193A in dsRBD2 are represented by “mut.”

simultaneously and in the same manner as the first binding mode, which might explain why the affinity of the second binding mode is much lower than that of the first binding mode.

Dimer dissociation analysis of the full-length TRBP

The present ITC experiments indicated that TRBP binds siRNA as a monomer. On the other hand, TRBP reportedly forms dimers in solution.^{19,30} Therefore, we examined the dimerization of the full-length TRBP protein. First, we performed gel filtration chromatography experiments with various concentrations of protein solutions, from 0.5 to 40 μM [Fig. 5(A)]. The elution peak shifted backward at lower TRBP concentrations, indicating that the TRBP dimer dissociates into monomers at these concentrations. Next, we performed an analytical ultracentrifugation analysis. The TRBP solution, at a concentration of 38 μM , was analyzed by the sedimentation equilibrium method. The monomer–dimer equilibrium of TRBP, with a molecular mass of 38 kDa, gave a K_d value of 54 μM , whereas the molecular mass predicted using a single ideal species model was 52 kDa [Fig. 5(B)]. This large K_d value of 54 μM is consistent with the results from our gel filtration chromatography analysis. The present ITC measurements were performed at a concentration of around 1 μM , and the majority of the TRBP was monomeric.

Therefore, our finding that TRBP binds siRNA as a monomer is consistent with the weak dimerization of TRBP.

The hydrophobic residue in the L1 loop

Unlike dsRBD1, dsRBD2 has an extra tryptophan residue (Trp152) in the loop between the $\alpha 1$ helix and the $\beta 1$ strand [the L1 loop; Figs. 1(B) and 6(A–D)]. The side chain of Trp152 protrudes into the hydrophobic pocket consisting of Lys150, Glu178, Arg179, Phe180, and Val204. These interactions involve cation- π interactions²⁴ between the aromatic ring of Trp152 and the positively charged side chain of Lys150. On the other hand, dsRBD1 has neither the Trp152 equivalent in the L1 loop nor the surrounding residues.

Similar interactions involving the tryptophan residue also exist in the second dsRBD (dsRBD2) of XIRBP, which is the TRBP homolog in *Xenopus laevis* [PDB ID: 1DI2, Fig. 6(E)]²⁵ and the dsRBD of *Aquifex aeolicus* RNase III [PDB ID: 1RC7, Fig. 6(F)].³¹ These interactions, which occur on the opposite side of the dsRNA-binding surface, seem to contribute to the stabilization of the domain structure.

We generated two substitution mutants, Trp152Ala and Trp152Val, and the Trp152-deleted mutant of the dsRBD2 fragment (D2-W152A, D2-W152V, and D2-W152del, respectively). We examined the CD spectra of the three mutant dsRBD2

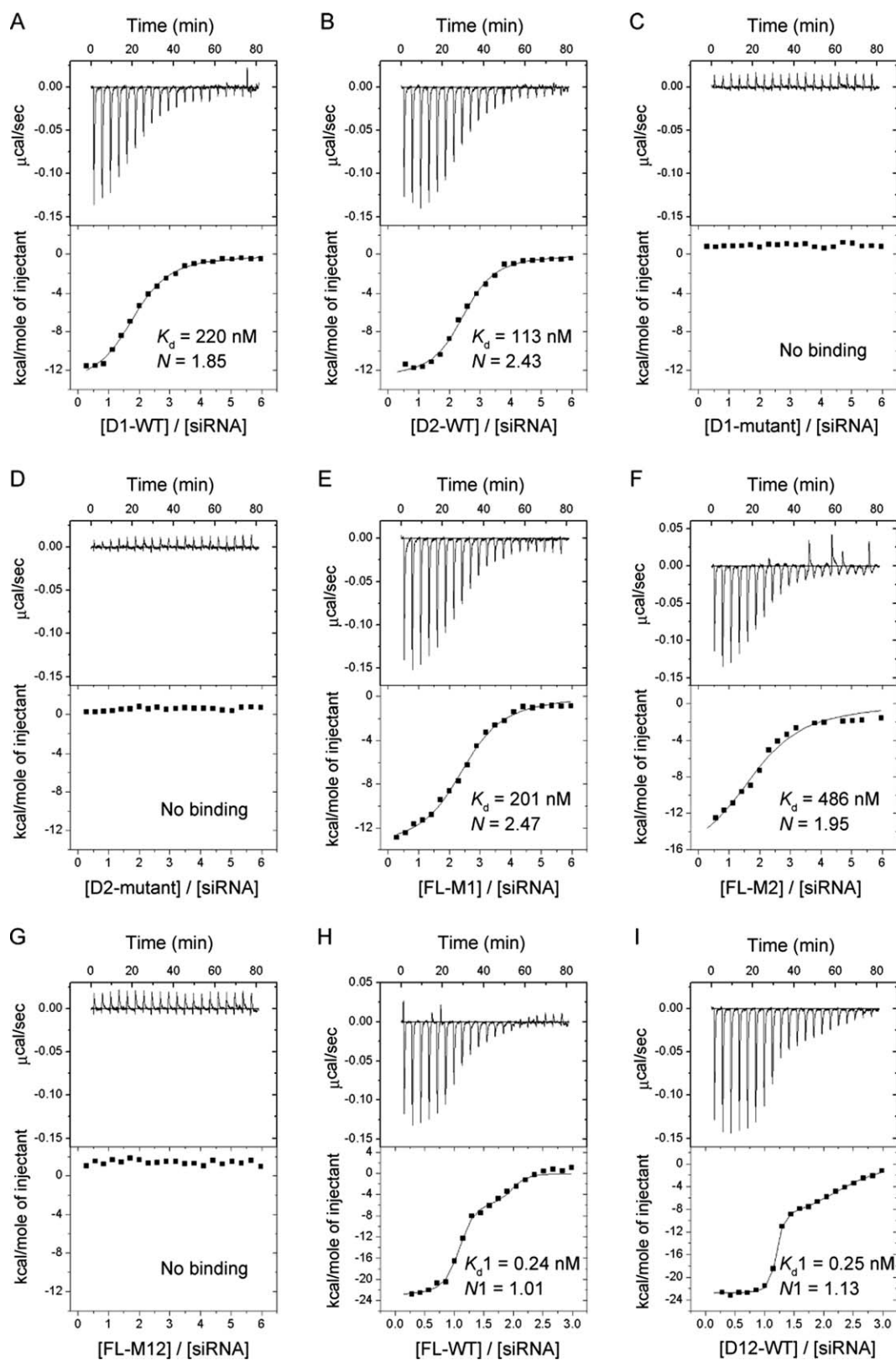


Figure 4. Binding patterns of the TRBP constructs. The heat change profiles of D1-WT (A), D2-WT (B), D1-mutant (C), D2-mutant (D), FL-M1 (E), FL-M2 (F), FL-M12 (G), FL-WT (H), and D12-WT (I). For each measurement, the upper panel shows the differential power versus time and the lower panel shows the integrated heats of the injections. The fitting-curves and the binding parameters are also indicated (K_d : dissociation constant, N : stoichiometry factor).

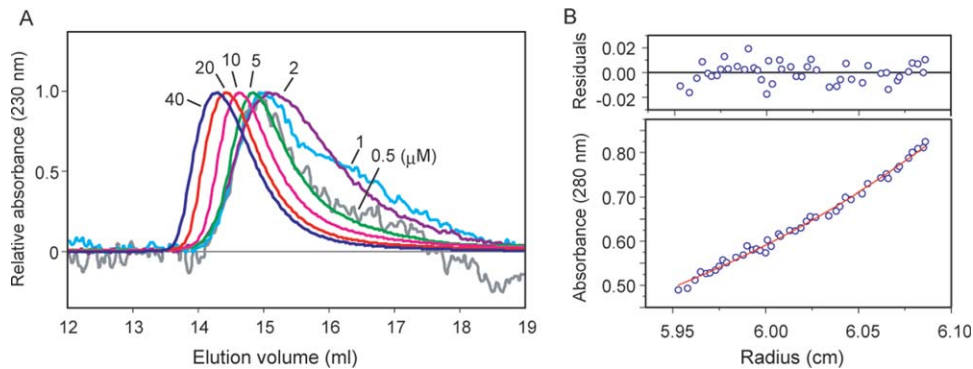


Figure 5. Dimer dissociation analysis of the full-length TRBP. (A) Gel filtration chromatography profiles. The normalized absorbances at 230 nm are shown with the injectant concentrations (μM). (B) Analytical ultracentrifugation plots. The plot of the sedimentation equilibrium data at 10,000 rpm is shown. The solid line in the lower panel corresponds to the fit of the experimental data to the monomer–dimer equilibrium model. The upper panel shows the differences between the fitted curve and the experimental values.

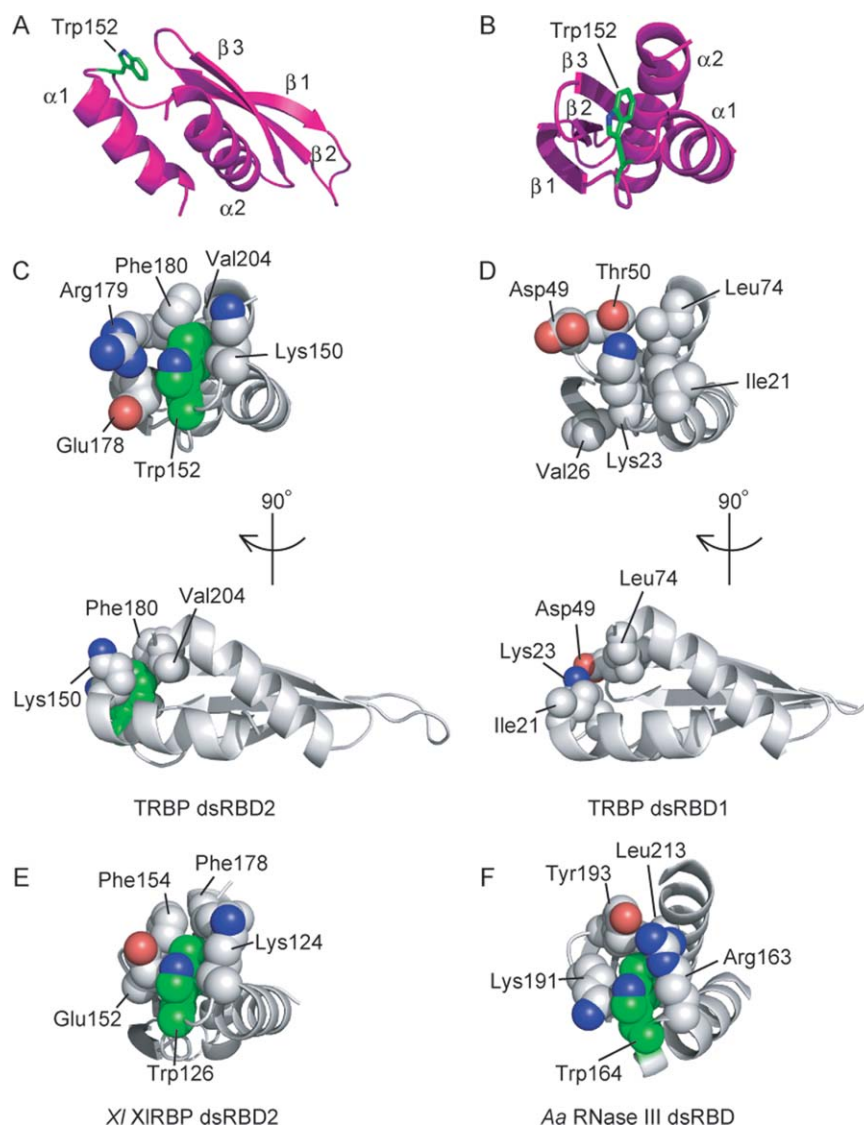


Figure 6. The hydrophobic residues in the L1 loop. (A, B) The position of Trp152 in TRBP dsRBD2. Trp152 is colored green. (C–F) Interactions involving Trp152 or its equivalent residues. The structures of the TRBP dsRBD2 (C, PDB ID: 2CPN), the human TRBP dsRBD1 (D, PDB ID: 3LLH), the *X. laevis* XIRBP dsRBD²⁵ (E, PDB ID: 1DI2), and the *A. aeolicus* RNase III dsRBD³¹ (F, PDB ID: 1RC7) are shown. The Trp152 residue or its equivalent (green), and the surrounding residues (gray) are represented by sphere models. An [interactive view](#) is available in the electronic version of the article.

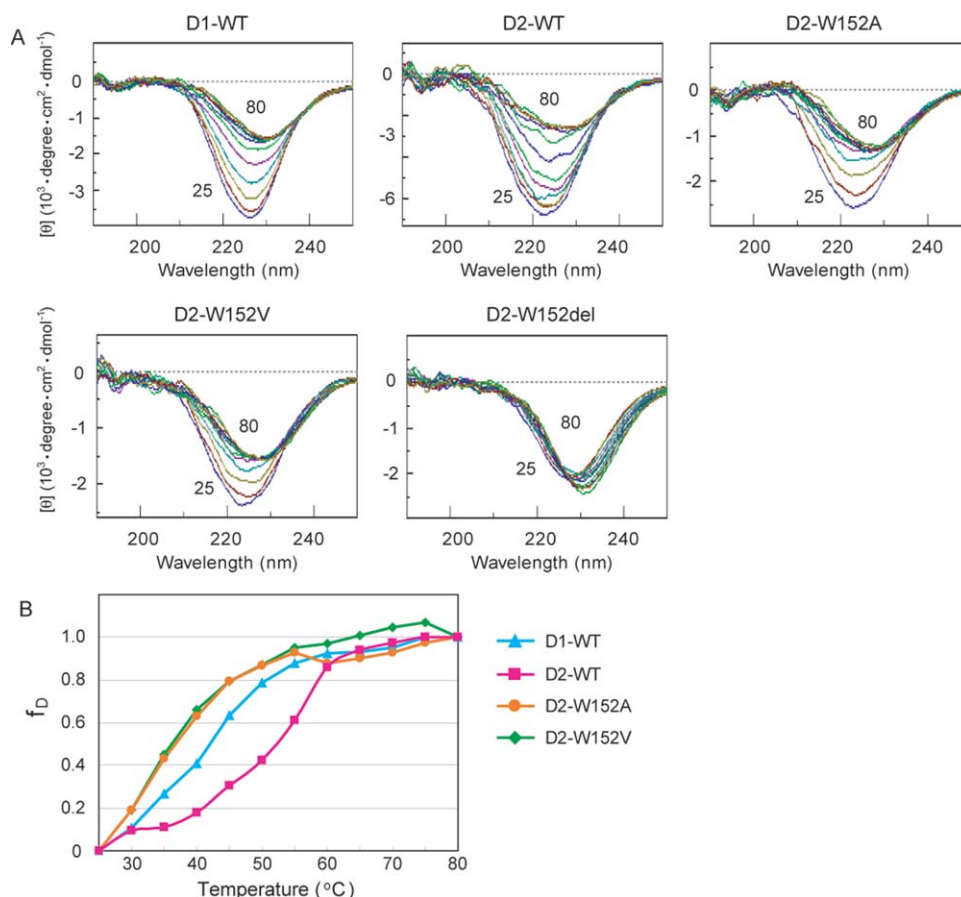


Figure 7. CD spectroscopy of the dsRBD fragments. (A) The far-UV CD spectra of the dsRBD fragments. The spectra measured at every 5 degrees from 25 to 80°C are superposed. (B) Denaturation curves of D1-WT (cyan closed triangles), D2-WT (magenta squares), D2-W152A (orange circles), and D2-W152V (green open triangles). The normalized ellipticities at 222 nm are plotted as a function of temperature.

fragments, as well as the wild-type dsRBD1 and dsRBD2 fragments (D1-WT and D2-WT, respectively), while raising the temperature from 25 to 80°C. The peak intensities around 222 nm of D1-WT, D2-WT, D2-W152A, and D2-W152V decreased as the temperature increased. On the other hand, the peak intensity of D2-W152del did not significantly change throughout the measurement, indicating that D2-W152del was unfolded at 25°C. We compared the stability of the proteins with the denaturation curves [Fig. 7(B)]. D2-WT denatured at a much higher temperature than D1-WT. The D2-W152A and D2-W152V mutants were unfolded even at lower temperatures than D1-WT. Taken together, these results indicate that dsRBD2 is more thermostable than dsRBD1, depending on the Trp residue.

We obtained the dsRBD sequences from the Pfam database³² and examined the hydrophobic residues at these positions. Among the 113 sequences grouped as the seed sequences (the representative members of the family) of DSRM (double-stranded RNA recognition motif), 10 sequences have Trp and 8 sequences have Phe at the corresponding positions [Fig. 8(A)]. One of the sequences with the Trp is the TRBP dsRBD2 homolog in *Danio rerio* (95.4% iden-

tity). Interestingly, the Trp residue is strongly correlated with Arg or Lys at the prior position, whereas Phe lacks such a detectable correlation. This preference may reflect the importance of the cation- π interaction between Trp and Lys/Arg, as the cation- π interaction with Phe is weaker than that with Trp.³³ Next, we prepared the phylogenetic tree consisting of TRBP dsRBD1, TRBP dsRBD2, and the 113 dsRBDs from the Pfam database. As shown in Figure 8(B), the dsRBDs with the Trp residue are widely and sporadically distributed. Therefore, the presence of these hydrophobic residues in the L1 loop may be a consequence of convergent evolution.

In this study, we solved the structures of dsRBD1 and dsRBD2 from human TRBP. The characteristic Trp residue in dsRBD2 contributes to its higher thermostability, when compared with that of dsRBD1. On the other hand, the two dsRBDs share similar dsRNA binding surfaces, with well-conserved residues, and dsRBD1 and dsRBD2 exhibited similar binding affinities for siRNA. This observation is in sharp contrast to the vastly different affinities between the two dsRBDs reported for the TAR RNA. The two dsRBDs in the full-length TRBP bind simultaneously to a single siRNA molecule, which results

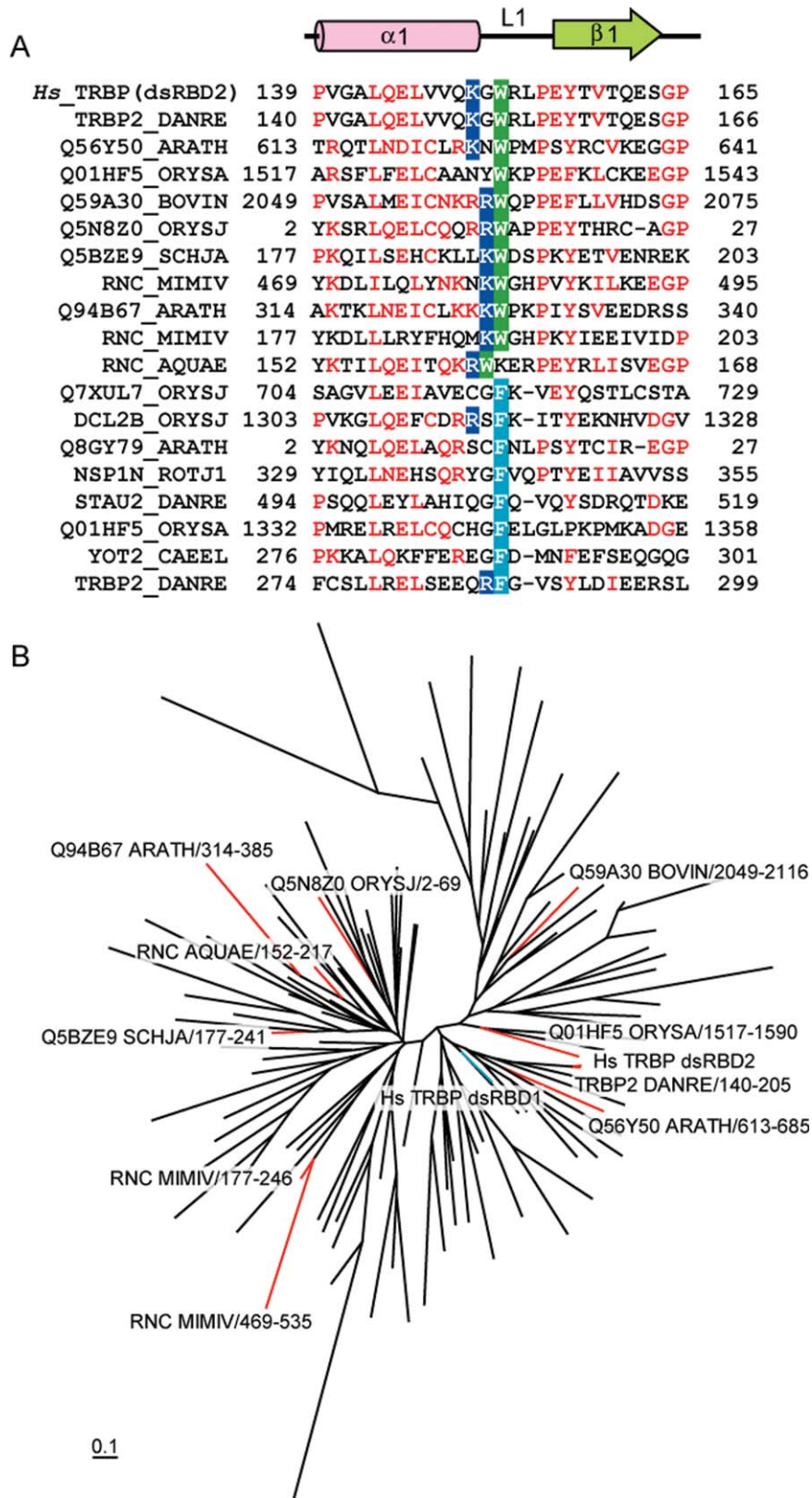


Figure 8. Sequence analysis of the dsRBDs with the Trp152 equivalents. (A) Sequence alignment of the dsRBDs with Trp or Phe at the positions corresponding to that of Trp152 in the human TRBP dsRBD2. These Trp and Phe residues are shaded in green and cyan, respectively. The Lys/Arg residues at the position prior to the Trp or Phe residue are shaded in blue. (B) Phylogenetic tree of the dsRBDs. The sequences were aligned using Clustal W³⁴ and adjusted manually. The phylogenetic tree was produced by TreeView.³⁵ The branches leading to the dsRBDs with the Trp residue (including TRBP dsRBD2) and that leading to the TRBP dsRBD1 are colored red and cyan, respectively.

in the subnanomolar dissociation constant. It will be interesting to study how siRNA is transferred from TRBP to Argonaute, on the basis of the siRNA binding properties of the tandem dsRBDs of TRBP.

Materials and Methods

X-ray sample preparation

The cDNA fragment encoding the TRBP dsRBD1 (residues 1–84) was cloned into the pGEX-6P plasmid (GE Healthcare). The dsRBD1 was expressed with a GST-tag, a precession protease cleavage site and a Leu-Gly-Ser-His sequence at the N-terminus. For overexpression, *E. coli* strain Rosetta(DE3) (Novagen) was used as the host. After lysis by sonication, the protein was isolated by GST affinity chromatography, and then the GST-tag was removed by proteolysis. Subsequent cation-exchange chromatography and size exclusion chromatography yielded the highly purified dsRBD1. The dsRBD1 sample for crystallization was concentrated to 6.0 mg ml⁻¹ in 20 mM Mes-NaOH buffer (pH 6.0), containing 100-mM NaCl and 1-mM DTT. The crystal used for data collection was obtained by mixing 0.7 μL of the dsRBD1 solution and 0.7 μL of the reservoir solution [1.44M sodium malonate (pH 7.0; Hampton Research), 200 mM AmsO₄, and 0.5% isopropanol]. Crystals were grown by the sitting-drop vapor-diffusion method at 293 K.

X-ray structure determination

For data collection, the crystals were harvested, soaked in 3.0M sodium malonate (pH 7.0), and flash-cooled in a liquid nitrogen stream. The data set was collected at the beamline NW12A of the Photon Factory (Tsukuba, Japan), and was processed with HKL2000.³⁶ The dsRBD1 crystal belonged to the space group *P*3₁, with unit cell parameters of *a* = *b* = 51.2 Å, *c* = 42.8 Å. The initial phase was solved by the molecular replacement method with Phaser,³⁷ using the polyalanine model of the *Aquifex aeolicus* RNase III structure (PDB ID: 1RC7, residues 151–220) as the search model. The polyalanine model was generated by MOLEMAN2.³⁸ The remainder of the structure was built automatically with ARP/wARP³⁹ and modified manually with Coot.⁴⁰ The refinement was performed with Refmac and CNS⁴¹ to 2.14 Å resolution. The *R*_{work} and *R*_{free} values were converged to 18.5 and 23.3%, respectively. The crystallographic asymmetric unit contained two dsRBD1 molecules, which were similar to each other, with an RMSD of 0.3 Å for 62 C^α atoms. The RMSDs were calculated by Superpose.⁴² Some residues were invisible because of disorder, and the final model includes residues Gly7–Glu33 and Pro39–Lys75 in the A chain and Gly7–Gly34 and Gln38–Lys75 in the B chain. The quality of the structures was analyzed using PROCHECK.⁴³

Table I. Structural Statistics of the dsRBD1 of TRBP

Native	
Data collection	
Space group	<i>P</i> 3 ₁
Cell constant (Å)	<i>a</i> = <i>b</i> = 51.2, <i>c</i> = 42.4
Wavelength (Å)	1.00000
Resolution range (Å) ^a	50–2.14 (2.22–2.14)
Reflections	6917
Completeness ^a	100 (100)
<i>R</i> _{merge} ^{a,b}	0.152 (0.807)
<i>I</i> / <i>σ</i> ^a	12.2 (2.3)
Redundancy ^a	5.8 (5.7)
Structural refinement	
Total protein atoms	985
Total solvent atoms	40
Resolution range (Å)	44.3–2.14
<i>R</i> _{work} ^b (%)	18.5
<i>R</i> _{free} ^b (%)	23.3
RMSD from ideality	
Bond lengths (Å)	0.0069
Bond angles (°)	1.2
Ramachandran plot ^c	
Residues in most-favored regions (%)	94.3
Residues in additionally allowed regions (%)	5.7
Residues in generously allowed regions (%)	0.0
Residues in disallowed regions (%)	0.0

^a $R_{\text{merge}} = \sum |I_{\text{av}} - I_i| / \sum I_i$, where I_{av} is the average of all individual observations I_i . Values in parentheses are for the highest-resolution shell.

^b $R_{\text{work/free}} = \sum |F_o - F_c| / \sum F_o$, where the crystallographic *R*-factor is calculated including and excluding refinement reflections. In each refinement, free reflections consist of 5% of the total number of reflections.

^c From PROCHECK.

Details of the experimental data and the structural statistics are summarized in Table I.

NMR sample preparation

The cDNA fragment encoding the TRBP dsRBD2 (residues 129–204) was cloned into the pCR2.1 vector (Invitrogen). The dsRBD2 was expressed with a His6-tag, a TEV protease cleavage site, a (Gly-Gly-Ser)₂-Gly sequence at the N-terminus and a Ser-Gly-Pro-Ser-Ser-Gly sequence at the C-terminus. The ¹⁵N, ¹³C-labeled TRBP dsRBD2 used for NMR experiments was synthesized by the cell-free protein expression system.⁴⁴ After the reaction, the protein was isolated by Ni affinity chromatography, and then the His6-tag was removed by proteolysis. Subsequent cation-exchange chromatography yielded the highly purified dsRBD2. The TRBP dsRBD2 sample for NMR experiments was concentrated to 1.15 mM in 20 mM Tris-HCl buffer (pH 7.0), containing 100 mM NaCl, 1 mM DTT, and 0.02% NaN₃ in 90% H₂O–10% ²H₂O.

NMR spectroscopy

Triple resonance spectra were recorded at 298 K on a Bruker AVANCE 700-MHz NMR spectrometer.

NMR spectra were processed with NMRPipe/NMRDraw.⁴⁵ Spectral analysis was performed with KUIJIRA,⁴⁶ a program suite for interactive NMR analysis working with NMRView,⁴⁷ according to the methods described previously.⁴⁸ Backbone and side-chain ¹H, ¹⁵N, and ¹³C resonances of the proteins were assigned by standard double- and triple-resonance NMR experiments.^{49–51} Distance restraints were derived from three-dimensional (3D) ¹⁵N-separated and ¹³C-separated nuclear Overhauser effect spectroscopy (NOESY)-HSQC spectra, each measured with a mixing time of 80 ms.

NMR structure calculations

Structure calculations of the TRBP dsRBD2 were performed using the program CYANA2.0.17.^{52–54} The structure calculations started from 100 randomized conformers and used the standard CYANA simulated annealing schedule, with 15,000 torsion angle dynamics steps per conformer. The 20 conformers with the lowest final CYANA target function values were subjected to restrained energy minimization in implicit solvent (generalized Born solvation model) with the program AMBER9, using the AMBER 2003 force field.⁵⁵ The number of energy minimization steps was 2,000. Force constants of 32 kcal mol⁻¹ Å⁻² for distance restraints, 60 kcal mol⁻¹ rad⁻² for torsion angle restraints and 50 kcal mol⁻¹ rad⁻² for ω angles were used in the energy minimization. The 20 lowest energy conformers were then used for further analyses. The quality of the structures was analyzed using PROCHECK-NMR.⁵⁶ Detailed experimental data and structural statistics are summarized in Table II.

Sample preparation for the biochemical analyses

The sequences of the chemically synthesized siRNAs (Takara Bio) were 5'-UGAGGUAGUAGGUUGUAUAGU-3' and 5'-UAUACAACCUACUACCUCAUU-3'.

The cDNA fragments encoding the full-length TRBP (residues 1–345), the dsRBD1 fragment (residues 1–84), the dsRBD2 fragment (residues 121–213), and the dsRBD3-deleted fragment (residues 1–213) were cloned into pCold II (Takara Bio). The mutants were generated with a QuikChange mutagenesis kit (Stratagene) or by the overlap PCR method. The proteins were expressed with a Met-Asn-His-Lys-Val sequence and a His6-tag at the N-terminus. The dsRBD2 fragments contain an extra Met residue derived from the vector sequence just after the His6-tag. For overexpression, *E. coli* strain Rosetta(DE3) was used as the expression host. After lysis by sonication, the proteins were isolated by Ni affinity chromatography and subsequent cation-exchange chromatography. The D1-WT, D2-WT, FL-WT, FL-M1, FL-M2, D12-WT, D2-W152A, D2-W152V, and D2-W152del proteins were further purified by heparin

Table II. Structural Statistics of the dsRBD2 of TRBP

Wild-type	
Constraints for final structure calculations	
No. of NOE distance restraints	1239
Intraresidue	0
Sequential ($ i - j = 1$)	655
Medium range ($1 < i - j < 5$)	222
Long range ($ i - j \geq 5$)	362
No. of dihedral angle restraints ^a	
φ angles	52
ψ angles	50
χ angles	25
No. of hydrogen bond restraints ^b	34
Ensemble statistics (20 structures)	
Mean number of NOE violations > 0.2 Å	0
Mean number of dihedral angle violations > 3°	0
Average CYANA target function (Å ²)	0.0104 ± 0.0029
Energies of AMBER calculation	
Mean AMBER energy (kcal/mol)	-2771.5430
Mean restraint violation energy (kcal/mol)	6.062
RMS deviation to mean coordinates ^c	
Backbone heavy atoms (Å)	0.32 ± 0.08
All heavy atoms (Å)	1.13 ± 0.17
Ramachandran plot ^d	
Residues in most-favored regions (%)	96.5
Residues in additionally allowed regions (%)	3.5
Residues in generously allowed regions (%)	0.0
Residues in disallowed regions (%)	0.0

^a φ and ψ angles were derived from the program TALOS, based on the ¹³C^α, ¹³C^β, ¹³CO, ¹H^α, and ¹⁵N chemical shifts. The χ angles contain 16 χ₁ and 9 χ₂ angle restraints for both proteins.

^b Only hydrogen bonds supported by NOEs are used.

^c Residues Val140–Val204 were used.

^d From PROCHECK-NMR for 20 models. Residues Val140–Val204 were used.

affinity chromatography. The purified proteins were dialyzed against 20 mM Hepes-NaOH buffer (pH 7.5), containing 150 mM NaCl and 1 mM DTT.

ITC measurements

ITC measurements were performed with a VP-ITC calorimeter (GE Healthcare) at 25°C. Samples were buffered with 20 mM Hepes-NaOH buffer (pH 7.5), containing 150 mM NaCl. Aliquots of 40 μM (D1-WT, D2-WT, D1-mutant, D2-mutant, FL-M1, FL-M2, and FL-M12) or 20 μM (FL-WT and D12-WT) protein solutions (syringe) were stepwise injected into a 1 μM siRNA solution (cell). The data were analyzed with the Origin software (Microcal). The heat generated due to the dilution of the protein solutions was quite small and was ignored for the analysis. A one-site binding model was used for the analysis of D1-WT, D2-WT, FL-M1, and FL-M2. On the other hand, a two-site binding model was used for the analysis of FL-WT and D12-WT.

Gel filtration chromatography

Gel filtration chromatography was performed with a Superdex 200 10/30 column (GE Healthcare) at 4°C. The samples were buffered with 20 mM Hepes-NaOH buffer (pH 7.5), containing 150 mM NaCl and 1 mM DTT. For each analysis, a 200- μ L aliquot of the protein solution was injected and the absorbance at 230 nm was monitored.

Analytical ultracentrifugation

Analytical ultracentrifugation was performed by the sedimentation equilibrium method. The 38 μ M TRBP solution was analyzed with an Optima XL-I analytical ultracentrifuge (Beckman Coulter) at 20°C. The sample was buffered in 20 mM Hepes-NaOH buffer (pH 7.5), containing 150 mM NaCl and 1 mM DTT. The solvent density and the viscosity were calculated with SEDNTERP.⁵⁷ The protein distributions were monitored at 280 nm. The equilibrium data were obtained at 8,000, 9,000, and 10,000 rpm and were fitted using the Origin software (Microcal).

CD spectroscopy

CD spectroscopy was performed with a J-820 spectrometer equipped with a Peltier temperature control system (JASCO), using 15–50 μ M protein solutions. The spectra were recorded with three accumulations at every 5 degrees from 25 to 80°C, after 1-min incubation at each target temperature.

Protein Data Bank accession codes

The coordinates and structure factors for the TRBP dsRBD1 and the 20 energy-minimized conformers of the TRBP dsRBD2 have been deposited in the Protein Data Bank (PDB), with the accession codes 3LLH and 2CPN, respectively.

Acknowledgments

The authors are grateful to E. Seki for gene cloning, M. Inoue, Y. Tomo, T. Yabuki, and M. Aoki for sample screening, T. Matsuda, N. Matsuda, Y. Motoda, and Y. Fujikura for cell-free protein expression, and Y. Tomabechi for large-scale preparation of the samples for NMR analysis. The authors are grateful to R. Akasaka for the ultracentrifugation analysis, and T. Kasai for advice on ITC measurements.

References

1. Siomi H, Siomi MC (2009) On the road to reading the RNA-interference code. *Nature* 457:396–404.
2. Bernstein E, Caudy AA, Hammond SM, Hannon GJ (2001) Role for a bidentate ribonuclease in the initiation step of RNA interference. *Nature* 409:363–366.
3. Provost P, Dishart D, Doucet J, Frenthewey D, Samuelsson B, Rådmark O (2002) Ribonuclease activity and RNA binding of recombinant human Dicer. *EMBO J* 21:5864–5874.
4. Zhang H, Kolb FA, Brondani V, Billy E, Filipowicz W (2002) Human Dicer preferentially cleaves dsRNAs at

their termini without a requirement for ATP. *EMBO J* 21:5875–5885.

5. Matranga C, Tomari Y, Shin C, Bartel DP, Zamore PD (2005) Passenger-strand cleavage facilitates assembly of siRNA into Ago2-containing RNAi enzyme complexes. *Cell* 123:607–620.
6. Leuschner PJ, Ameres SL, Kueng S, Martinez J (2006) Cleavage of the siRNA passenger strand during RISC assembly in human cells. *EMBO Rep* 7:314–320.
7. Hammond SM, Boettcher S, Caudy AA, Kobayashi R, Hannon GJ (2001) Argonaute2, a link between genetic and biochemical analyses of RNAi. *Science* 293:1146–1150.
8. Rossi JJ (2005) Mammalian Dicer finds a partner. *EMBO Rep* 6:927–929.
9. Chendrimada TP, Gregory RI, Kumaraswamy E, Norman J, Cooch N, Nishikura K, Shiekhattar R (2005) TRBP recruits the Dicer complex to Ago2 for microRNA processing and gene silencing. *Nature* 436:740–744.
10. Haase AD, Jaskiewicz L, Zhang H, Lainé S, Sack R, Gagnon A, Filipowicz W (2005) TRBP, a regulator of cellular PKR and HIV-1 virus expression, interacts with Dicer and functions in RNA silencing. *EMBO Rep* 10:961–967.
11. Lee Y, Hur I, Park SY, Kim YK, Suh MR, Kim VN (2006) The role of PACT in the RNA silencing pathway. *EMBO J* 25:522–532.
12. Gagnon A, Buckler-White A, Berkhout B, Jeang KT (1991) Characterization of a human TAR RNA-binding protein that activates the HIV-1 LTR. *Science* 251:1597–1600.
13. Daviet L, Erard M, Dorin D, Duarte M, Vaquero C, Gagnon A (2000) Analysis of a binding difference between the two dsRNA-binding domains in TRBP reveals the modular function of a KR-helix motif. *Eur J Biochem* 267:2419–2431.
14. Gagnon A, Buckler C, Jeang KT (1993) Relatedness of an RNA-binding motif in human immunodeficiency virus type 1 TAR RNA-binding protein TRBP to human P1/dsI kinase and *Drosophila staufer*. *Mol Cell Biol* 13:2193–2202.
15. Parker GS, Maity TS, Bass BL (2008) dsRNA binding properties of RDE-4 and TRBP reflect their distinct roles in RNAi. *J Mol Biol* 384:967–979.
16. Kok KH, Ng MH, Ching YP, Jin DY (2007) Human TRBP and PACT directly interact with each other and associate with dicer to facilitate the production of small interfering RNA. *J Biol Chem* 282:17649–17657.
17. Ma E, MacRae IJ, Kirsch JF, Doudna JA (2008) Auto-inhibition of human dicer by its internal helicase domain. *J Mol Biol* 380:237–243.
18. Melo SA, Roper S, Moutinho C, Aaltonen LA, Yamamoto H, Calin GA, Rossi S, Fernandez AF, Carneiro F, Oliveira C, Ferreira B, Liu CG, Villanueva A, Capella G, Schwartz S, Jr, Shiekhattar R, Esteller M (2009) A TARBP2 mutation in human cancer impairs microRNA processing and DICER1 function. *Nat Genet* 41:365–370.
19. MacRae IJ, Ma E, Zhou M, Robinson CV, Doudna JA (2008) In vitro reconstitution of the human RISC-loading complex. *Proc Natl Acad Sci USA* 105:512–517.
20. Liu Q, Rand TA, Kalidas S, Du F, Kim HE, Smith DP, Wang X (2003) R2D2, a bridge between the initiation and effector steps of the *Drosophila* RNAi pathway. *Science* 301:1921–1925.
21. Wang HW, Noland C, Siridechadilok B, Taylor DW, Ma E, Felderer K, Doudna JA, Nogales E (2009) Structural insights into RNA processing by the human RISC-loading complex. *Nat Struct Mol Biol* 16:1148–1153.
22. Yang SW, Chen HY, Yang J, Machida S, Chua NH, Yuan YA (2010) Structure of Arabidopsis HYPONASTIC

- LEAVES1 and its molecular implications for miRNA processing. *Structure* 18:594–605.
23. Doyle M, Jantsch MF (2002) New and old roles of the double-stranded RNA-binding domain. *J Struct Biol* 140:147–153.
 24. Dougherty DA (1996) Cation- π interactions in chemistry and biology: a new view of benzene, Phe, Tyr, and Trp. *Science* 271:163–168.
 25. Rytter JM, Schultz SC (1998) Molecular basis of double-stranded RNA-protein interactions: structure of a dsRNA-binding domain complexed with dsRNA. *EMBO J* 17:7505–7513.
 26. Sohn SY, Bae WJ, Kim JJ, Yeom KH, Kim VN, Cho Y (2007) Crystal structure of human DGCR8 core. *Nat Struct Mol Biol* 14:847–853.
 27. Stefl R, Xu M, Skrisovska L, Emeson RB, Allain FH (2006) Structure and specific RNA binding of ADAR2 double-stranded RNA binding motifs. *Structure* 14:345–355.
 28. Bycroft M, Grünert S, Murzin AG, Proctor M, St Johnston D (1995) NMR solution structure of a dsRNA binding domain from *Drosophila staufer* protein reveals homology to the N-terminal domain of ribosomal protein S5. *EMBO J* 14:3563–3571.
 29. Ramos A, Grünert S, Adams J, Micklem DR, Proctor MR, Freund S, Bycroft M, St Johnston D, Varani G (2000) RNA recognition by a Staufen double-stranded RNA-binding domain. *EMBO J* 19:997–1009.
 30. Cosentino GP, Venkatesan S, Serluca FC, Green SR, Mathews MB, Sonenberg N (1995) Double-stranded-RNA-dependent protein kinase and TAR RNA-binding protein form homo- and heterodimers in vivo. *Proc Natl Acad Sci USA* 92:9445–9449.
 31. Blaszczyk J, Gan J, Tropea JE, Court DL, Waugh DS, Ji X (2004) Noncatalytic assembly of ribonuclease III with double-stranded RNA. *Structure* 12:457–466.
 32. Bateman A, Birney E, Cerruti L, Durbin R, Ewinger L, Eddy SR, Griffiths-Jones S, Howe KL, Marshall M, Sonnhammer EL (2002) The Pfam protein families database. *Nucleic Acids Res* 30:276–280.
 33. Shi Z, Olson CA, Kallenbach NR (2002) Cation- π interaction in model α -helical peptides. *J Am Chem Soc* 124:3284–3291.
 34. Thompson JD, Higgins DG, Gibson TJ (1994) CLUSTAL W: improving the sensitivity of progressive multiple sequence alignment through sequence weighting, position-specific gap penalties and weight matrix choice. *Nucleic Acids Res* 22:4673–4680.
 35. Page RD (2002) Visualizing phylogenetic trees using TreeView. *Curr Protoc Bioinformatics* Chapter 6:Unit 6.2.
 36. Otwinowski Z, Minor W (1997) Processing of X-ray diffraction data collected in oscillation mode. *Methods Enzymol* 276:307–326.
 37. McCoy AJ, Grosse-Kunstleve RW, Adams PD, Winn MD, Storoni LC, Read RJ (2007) Phaser crystallographic software. *J Appl Crystallogr* 40:658–674.
 38. Kleywegt GJ (1996) Making the most of your search model. *CCP4/ESF-EACBM Newsletter on Protein Crystallogr* 32:32–36.
 39. Perrakis A, Morris R, Lamzin VS (1999) Automated protein model building combined with iterative structure refinement. *Nat Struct Biol* 6:458–463.
 40. Emsley P, Cowtan K (2004) Coot: model-building tools for molecular graphics. *Acta Crystallogr D Biol Crystallogr* 60:2126–2132.
 41. Brünger AT, Adams PD, Clore GM, DeLano WL, Gros P, Grosse-Kunstleve RW, Jiang JS, Kuszewski J, Nilges M, Pannu NS, Read RJ, Rice LM, Simonson T, Warren GL (1998) Crystallography & NMR system: a new software suite for macromolecular structure determination. *Acta Crystallogr D Biol Crystallogr* 54:905–921.
 42. Diamond R (1992) On the multiple simultaneous superposition of molecular structures by rigid body transformations. *Protein Sci* 1:1279–1287.
 43. Laskowski RA, Moss DS, Thornton JM (1993) Main-chain bond lengths and bond angles in protein structures. *J Mol Biol* 231:1049–1067.
 44. Matsuda T, Koshiba S, Tochio N, Seki E, Iwasaki N, Yabuki T, Inoue M, Yokoyama S, Kigawa T (2007) Improving cell-free protein synthesis for stable-isotope labeling. *J Biomol NMR* 37:225–229.
 45. Delaglio F, Grzesiek S, Vuister GW, Zhu G, Pfeifer J, Bax A (1995) NMRPipe: a multidimensional spectral processing system based on UNIX pipes. *J Biomol NMR* 6:277–293.
 46. Kobayashi N, Iwahara J, Koshiba S, Tomizawa T, Tochio N, Güntert P, Kigawa T, Yokoyama S (2007) KIJIRA, a package of integrated modules for systematic and interactive analysis of NMR data directed to high-throughput NMR structure studies. *J Biomol NMR* 39:31–52.
 47. Johnson BA, Blevins RA (1994) NMRView: a computer program for the visualization and analysis of NMR data. *J Biomol NMR* 4:604–613.
 48. Nagata T, Suzuki S, Endo R, Shirouzu M, Terada T, Inoue M, Kigawa T, Kobayashi N, Güntert P, Tanaka A, Hayashizaki Y, Muto Y, Yokoyama S (2008) The RRM domain of poly(A)-specific ribonuclease has a non-canonical binding site for mRNA cap analog recognition. *Nucleic Acids Res* 36:4754–4767.
 49. Clore GM, Gronenborn AM (1998) Determining the structures of large proteins and protein complexes by NMR. *Trends Biotechnol* 16:22–34.
 50. Bax A (1994) Multidimensional nuclear magnetic resonance methods for protein studies. *Curr Opin Struct Biol* 4:738–744.
 51. Cavanagh J, Fairbrother WJ, Palmer AG, III, Skelton NJ (1996) *Protein NMR spectroscopy, principles and practice*. San Diego: Academic Press.
 52. Güntert P (2004) Automated NMR structure calculation with CYANA. *Methods Mol Biol* 278:353–378.
 53. Güntert P, Mumenthaler C, Wüthrich K (1997) Torsion angle dynamics for NMR structure calculation with the new program DYANA. *J Mol Biol* 273:283–298.
 54. Herrmann T, Güntert P, Wüthrich K (2002) Protein NMR structure determination with automated NOE assignment using the new software CANDID and the torsion angle dynamics algorithm DYANA. *J Mol Biol* 319:209–227.
 55. Duan Y, Wu C, Chowdhury S, Lee MC, Xiong G, Zhang W, Yang R, Cieplak P, Luo R, Lee T, Caldwell J, Wang J, Kollman P (2003) A point-charge force field for molecular mechanics simulations of proteins based on condensed-phase quantum mechanical calculations. *J Comput Chem* 24:1999–2012.
 56. Laskowski RA, Rullmann JA, MacArthur MW, Kaptein R, Thornton JM (1996) AQUA and PROCHECK-NMR: programs for checking the quality of protein structures solved by NMR. *J Biomol NMR* 8:477–486.
 57. Laue TM, Shah B, Ridgeway TM, Pelletier SL (1992) *Analytical Ultracentrifugation in Biochemistry and Polymer Science*. London: Royal Society of Chemistry, pp 90–125.